Journal of Environmental Management 114 (2013) 362–371

Contents lists available at SciVerse ScienceDirect

Journal of Environmental Management

journal homepage: www.elsevier.com/locate/jenvman

Assessing the impacts of droughts on net primary productivity in China

Fengsong Pei, Xia Li*, Xiaoping Liu, Chunhua Lao

School of Geography and Planning, and Guangdong Key Laboratory for Urbanization and Geo-simulation, Sun Yat-sen University, 135 West Xingang Road, Guangzhou 510275, PR China

ARTICLE INFO

Article history:
Received 18 July 2012
Received in revised form
16 October 2012
Accepted 23 October 2012
Available online 17 November 2012

Keywords:
Drought
Net primary productivity
Standardized anomaly index
China

ABSTRACT

Frequency and severity of droughts were projected to increase in many regions. However, their effects of temporal dynamics on the terrestrial carbon cycle remain uncertain, and hence deserve further investigation. In this paper, the droughts that occurred in China during 2001–2010 were identified by using the standardized precipitation index (SPI). Standardized anomaly index (SAI), which has been widely employed in reflecting precipitation, was extended to evaluate the anomalies of net primary productivity (NPP). In addition, influences of the droughts on vegetation were explored by examining the temporal dynamics of SAI–NPP along with area-weighted drought intensity at different time scales (1, 3, 6, 9 and 12 months). Year-to-year variability of NPP with several factors, including droughts, NDVI, radiation and temperature, was analyzed as well.

Consequently, the droughts in the years 2001, 2006 and 2009 were well reconstructed. This indicates that SPI could be applied to the monitoring of the droughts in China during the past decade (2001–2010) effectively. Moreover, strongest correlations between droughts and NPP anomalies were found during or after the drought intensities reached their peak values. In addition, some droughts substantially reduced the countrywide NPP, whereas the others did not. These phenomena can be explained by the regional diversities of drought intensity, drought duration, areal extents of the droughts, as well as the cumulative and lag responses of vegetation to the precipitation deficits. Besides the drought conditions, normalized difference vegetation index (NDVI), radiation and temperature also contribute to the interannual variability of NPP.

1. Introduction

According to the inventory-based analysis (Goodale et al., 2002) and the findings of global carbon cycle modeling (Fan et al., 1998; Peylin et al., 2002), northern terrestrial ecosystems are functioning as a large carbon sink. The magnitude, distribution and causes of the carbon sink remain unclear. However, Recent studies argued that the northern terrestrial ecosystem takes up less carbon than thought before (Stephens et al., 2007), and that the carbon sink is weakening (Fung et al., 2005; Canadell et al., 2007). Furthermore, this natural ecosystem might be transformed from a carbon sink to a carbon source owing to some disturbances (Ciais et al., 2005; Kurz et al., 2008). Accordingly, understanding the responses of the terrestrial ecosystem to various ecological disturbances is crucial for elucidating the effects of climate change on carbon cycling and other ecosystem processes at regional to global scale (Kurz et al., 2008; Running, 2008).

An ecological disturbance is defined as a phenomenon of sustained disruption of ecosystem structure and function (Pickett and White, 1986). There are many kinds of disturbances, including physical disturbance, biogenic disturbance and anthropogenic disturbance (Potter et al., 2003). The effects of major disturbances such as fires, deforestation and urbanization on the terrestrial carbon cycle have been studied extensively (Houghton and Goodale, 2004; Xu et al., 2007; van der Werf et al., 2010). However, the influences of another kind of disturbance, which are frequently less intense but more extensive, such as droughts, are not well understood. Furthermore, a trend of dryness was inferred from the global climate models under the conditions of rising greenhouse gases concentrations (Gregory et al., 1997; Burke et al., 2006). Frequency and intensity of droughts were supposed to increase in many regions in the 21st century (IPCC, 2007). Although the severity of droughts has been investigated extensively, their subsequent influences on terrestrial carbon cycle are not well explored (Zeng et al., 2004).

Numerous issues concerning the consequences of droughts on terrestrial biosphere need to be addressed in future studies. In this study, we focus specifically on how droughts affect net

* Corresponding author. Tel.: +86 13924203023; fax: +86 20 84115833.
E-mail addresses: lixia@graduate.hku.hk, lixia@mail.sysu.edu.cn (X. Li).
URL: http://www.geosimulation.cn/

0301-4797/$ – see front matter © 2012 Elsevier Ltd. All rights reserved.
http://dx.doi.org/10.1016/j.jenvman.2012.10.031

primary productivity (NPP) of the landscapes. NPP pertains to the production of organic compounds from atmospheric or aquatic carbon dioxide (CO_2), principally through the process of photosynthesis (photosynthesis minus autotrophic respiration). As the foundation of energy flow and nutrient cycle for organisms, NPP plays an important role in the global carbon balance, as well as in climate change. In addition, the carbon flux between the terrestrial biosphere and atmosphere such as NPP is primarily dominated by solar radiation, precipitation and temperature, ambient CO_2 concentration, land cover, and other local environmental factors (Cramer et al., 1999). Thus, it is a difficult task to distinguish the contributions of these factors to the variability of NPP.

Europe-wide reduction in primary productivity, which was caused by heat and droughts in 2003, was investigated at a continental scale (Ciais et al., 2005). Most recent findings show that some of the large-scale droughts reduced global NPP accompanied with decreased NPP in the Southern Hemisphere and increased NPP in the Northern Hemisphere in the period 2000–2009 (Zhao and Running, 2010). At a local to regional scale, Xiao et al. (2009) examined how droughts affected the terrestrial carbon dynamics by using the Palmer drought severity index (PDSI) and Terrestrial Ecosystem Model (TEM). They concluded that most of the drought events occurred in China during the twentieth century reduced the NPP and net ecosystem productivity (NEP) in large parts of the drought-affected areas. Besides drought intensity, timing of droughts is crucial to the carbon uptake of terrestrial ecosystems as well. Arnone et al. (2008) reported a sustained decrease of ecosystem CO_2 uptake in both the anomalously warming year with a drought and the following years by performing a four-year study. Standardized precipitation index (SPI), one of the meteorological-drought indices based on precipitation, was utilized to quantify the droughts in Colorado at multiple time scales effectively (McKee et al., 1993). Ji and Peters (2003) assessed the vegetation responses to the droughts in the Northern Great Plains in the U.S. by using SPI and normalized difference vegetation index (NDVI). They found that the three months SPI (SPI-3) had the maximal correlations with the NDVI. However, Fernandes and Heinemann (2011) concluded that the SPI at the time scale of 12 months (SPI-12) exhibited the best performance when estimating the variability of upland rice adjusted yield in six different regions in Brazil.

The severity of droughts is often characterized by drought intensity and drought duration (Liu and Juárez, 2001). Most of the previous studies have quantified the impacts of drought intensity on terrestrial NPP. However, the potential delayed or lagged effects of droughts have not been well understood because of their complexities. Especially, China has witnessed numerous droughts at different time scales in past decades (Wu et al., 2011). These droughts have exerted an important influence on the carbon cycle at a countrywide scale (Xiao et al., 2009). In this paper, several droughts that occurred in China during the past decade (2001–2010) were identified by using SPI as the indicator. The impacts of the intensity and timing of these droughts on terrestrial NPP were investigated by using statistical analysis, such as correlation analysis. Year-to-year variability between NPP and several factors was analyzed as well. In brief, this paper aims to assess the impacts of the intensity and temporal variability of droughts on NPP in China.

2. Data and preprocessing

2.1. Measurement-based biomass and NPP data

In our study, forest biomass/NPP data which were used for calibrating the Carnegie-Ames-Stanford approach (CASA) model were derived from Luo's (1996) study. These data were compiled from the national forest inventories conducted by the Chinese Ministry of Forestry during the period 1989–1993, as well as some other published literatures from intensively studied and well-documented field sites. These data provide some useful information, such as site name, latitude, longitude, elevation, biomass and NPP estimations for most of the plant components (Luo, 1996). Biomass and NPP data for grassland and shrubland were obtained from several published works (Jin et al., 2007; Ni, 2004; Togtohyn and Ojima, 1996; Wang et al., 2011a,b; Yu et al., 2000). These data were selected because: (1) a series of measurements was made at intervals during the growing season within one year or more; (2) data on aboveground and belowground biomass are available. Consequently, the corresponding NPP were calculated based on the maximum and minimum biomass following the method of Ni (2004). Since most of the measurement-based records on biomass and NPP were provided in the unit of dry matter (DM), a conversion was performed from DM to carbon content (g C $m^{-2}\cdot year^{-1}$). This was implemented by applying a conversion factor of 0.5 for woody biomass (Myneni et al., 2001), and 0.45 for grassland and shrubland (Fang et al., 2007).

2.2. Remote sensing data

The NDVI images are required by the CASA model when calculating NPP. These data were from the MODIS monthly NDVI product (MOD13) with a spatial resolution of 1 km^2. This was provided by the EOS Data Gateway at the Land Processes Distributed Archive Center (http://lpdaac.usgs.gov/main.asp). The images were then aggregated to geographic grid cells at a resolution of $0.01 \times 0.01^\circ$ from their original sinusoidal projection by using the MODIS reprojection tool. In addition, Vegetation Health Index (VHI), which was used for validating the NPP anomalies, was obtained from the Center for Satellite Applications and Research (STAR). These data were developed based on the radiance observed by the Advanced Very High Resolution Radiometer (AVHRR).

2.3. Climate datasets from NMIC/CMA

The climate dataset employed in this work, which covers the period from 1980 to 2010, includes mean temperature, precipitation and solar radiation at a monthly scale across China. Specifically, historical records of temperature and precipitation were derived from 752 climatological stations. The radiation data were compiled from 122 solar radiation observation stations. All these data were provided by the Chinese National Metrological Information Center/China Meteorological Administration (NMIC/CMA). In order to assure the continuity and consistency, these data were validated by screening and eliminating the suspicious and missing records. In addition, the interpolation technique of kriging (Zhu et al., 2006) was applied to mapping of the spatial distribution of each climate factor from the station-based information at a resolution of $0.01 \times 0.01^\circ$.

2.4. Vegetation map and soil texture data

Spatial distributions of various vegetation types in China were generated from a vegetation map at a scale of 1:1,000,000 (Editorial Board of Vegetation Map of China, 2001). For driving the CASA model properly, original categories of this vegetation map were reclassified into several typical vegetation types (Zhu et al., 2006). Following Potter et al. (1993), the soil rooting depth for various forests were set to 2.0 m, and the others were assigned a rooting

depth of 1.0 m. In addition, the information on the soil texture is important in determining the soil water content, and hence NPP. The harmonized world soil database (HWSD), which was produced by the Food and Agriculture Organization of the United Nations (Freddy et al., 2008), provides some soil parameters including soil texture classes and the associated particle sizes. The soil data in this study were compiled from the subset of HWSD at a scale of 1:1,000,000.

2.5. Land use/cover data

During the past three decades, urban lands in China have increasingly expanded and encroached upon lots of arable lands since the economic reform in 1978 (Li, 1998; Weng, 2002). The land use/cover dataset for 2006 in China was developed based on the updating survey by each province in China. Urban area in China was extracted from this land use/cover dataset by using Geographic Information System (GIS). However, the reclassification of the land use data toward the natural vegetation does not suit the parameters and structures of the CASA model. Thus, the vegetation map above was used to obtain the distributions of original vegetation in this country instead.

3. Methods

3.1. SPI as the indicator of droughts

Extreme weather and climate events such as droughts have received increasing attentions in the past few years. Researchers have developed many methods to monitor the meteorological and the other types of droughts (Palmer and Bureau, 1965; McKee et al., 1993; Tsakiris and Vangelis, 2005). In most cases, droughts could be quantified effectively via various drought indices such as SPI and PDSI. SPI was originally developed and applied to the monitoring of the status of droughts at multiple time scales in Colorado (McKee et al., 1993). Many studies suggested that SPI was suitable for quantifying most of the drought events, including meteorological, hydrological and agricultural droughts (Lloyd Hughes and Saunders, 2002).

The SPI is calculated by fitting a probability density function to the frequency distribution of some historical precipitation, which is summed over a specific time scale for each location. The probability density function is then transformed into a standardized normal distribution with a mean of zero and variance of one. In this study, time series of monthly precipitation was modeled by using the gamma distribution. The probability density function of this distribution is defined as (Lloyd Hughes and Saunders, 2002):

$$g(x) = \frac{1}{\beta^{\alpha}\Gamma(\alpha)} X^{\alpha-1} e^{-x/\beta} \quad \text{when } x > 0 \tag{1}$$

where α is a shape parameter, β is a scale parameter, and x is the amount of precipitation. $\Gamma(\alpha)$ is the gamma function, which is defined as

$$\Gamma(\alpha) = \int_0^{\infty} y^{\alpha-1} e^{-y} \mathrm{d}y \tag{2}$$

Here, α and β are estimated as follows:

$$\widehat{\alpha} = \frac{1}{4A}\left(1 + \sqrt{1 + \frac{4A}{3}}\right) \tag{3}$$

Table 1
Drought classification by SPI values.

SPI value	Drought category
2.00 or more	Extremely wet
1.50 to 1.99	Severely wet
1.00 to 1.49	Moderately wet
0 to 0.99	Mildly wet
0 to −0.99	Mild drought
−1.00 to −1.49	Moderate drought
−1.50 to −1.99	Severe drought
−2 or less	Extreme drought

$$\widehat{\beta} = \frac{\overline{x}}{\widehat{\alpha}} \tag{4}$$

For n observations

$$A = \ln(\overline{x}) - \frac{\sum \ln(x)}{n} \tag{5}$$

The cumulative probability $G(x)$ of an observed amount of precipitation is given as:

$$G(x) = \int_0^x g(x)\mathrm{d}x = \frac{1}{\widehat{\beta}^{\widehat{\alpha}}\Gamma(\widehat{\alpha})} \int_0^x x^{\widehat{\alpha}} e - x/\widehat{\beta}\mathrm{d}x \tag{6}$$

The gamma distribution is undefined as $x = 0$, and $q = P(x = 0) > 0$, where $P(x = 0)$ is the probability of zero precipitation. Thus, the cumulative probability becomes:

$$H(x) = q + (1 - q)G(x) \tag{7}$$

The cumulative probability distribution $H(x)$ is then transformed into standard normal distribution to yield the SPI by using the methods of Abramowitz and Stegun (1964):

$$Z = \mathrm{SPI} = -\left(t - \frac{c_0 + c_1 + c_2 t^2}{1 + d_1 + d_2 t^2 + d_3 t^3}\right) \quad \text{for} \quad 0 < H(x) \le 0.5 \tag{8}$$

$$Z = \mathrm{SPI} = +\left(t - \frac{c_0 + c_1 + c_2 t^2}{1 + d_1 + d_2 t^2 + d_3 t^3}\right) \quad \text{for} \quad 0.5 < H(x) < 1 \tag{9}$$

where

$$t = \sqrt{\ln\left(\frac{1}{(H(x))^2}\right)} \quad \text{for } 0 < H(x) \le 0.5 \tag{10}$$

$$t = \sqrt{\ln\left(\frac{1}{(1 - H(x))^2}\right)} \quad \text{for} \quad 0.5 < H(x) < 1 \tag{11}$$

and

$$c_0 = 2.515517;\ c_1 = 0.802853;\ c_2 = 0.010328;\ d_1 = 1.432788;\ d_2 = 0.189269;\ d_3 = 0.001308 \tag{12}$$

A clear and detailed description to calculate the SPI can be found in Lloyd Hughes and Saunders (2002). While using SPI as an indicator, we supposed that a drought occurs when the SPI falls below zero (McKee et al., 1993). In addition, a positive SPI often indicates

more precipitation than the median value, whereas negative values indicate lesser precipitation. As shown in Table 1, the SPI drought classification proposed by Lloyd Hughes and Saunders (2002) was used to measure the severity of droughts.

3.2. CASA for the calculations of NPP

In the past few years, a wide range of models has been developed to evaluate the NPP (Potter et al., 1993; Sitch et al., 2003; Sato et al., 2007). Among these models, the CASA, one of the satellite-based models (Cramer et al., 1999), has been widely employed in evaluating the terrestrial NPP in United States (Lobell et al., 2002), in China (Piao et al., 2005), as well as at a global scale (Potter et al., 1993).

The CASA model requires the parameters of NDVI, temperature, precipitation, solar radiation and so on. In this model, NPP was calculated as the product of the amount of photosynthetically active radiation (PAR) absorbed by green vegetation (APAR) and the light use efficiency (ε) that the radiation is converted to plant biomass increment:

$$\mathrm{NPP}(x,t) = \mathrm{APAR} \times \varepsilon \tag{13}$$

where NPP(x,t) is the net primary productivity fixed by vegetation at a grid cell x in month t, and APAR is the amount of photosynthetic active radiation. APAR is calculated by using the data on solar surface irradiance (S) and the fraction of photosynthetic active radiation absorbed by green vegetation (FPAR). ε for each grid cell can be determined as the product of $\varepsilon_{\max}$, and scalars representing the availability of soil moisture (W) and the suitability of temperature (T_1,T_2). Thus, the NPP in location x and time t becomes:

$$\mathrm{NPP}(x,t) = S(x,t) \times \mathrm{FPAR} \times 0.5 \times \varepsilon^{*} \times T_1(x,t) \times T_2(x,t) \times W(x,t) \tag{14}$$

where the factor 0.5 accounts for the fact that approximately half of the incoming solar radiation is in the photosynthetic active radiation waveband (0.4–0.7 μm). FPAR is defined as a linear function of the NDVI simple ratio. $\varepsilon_{\max}$ is determined by a calibration with field data from Luo's (1996) study. The details of the CASA model can be found in the studies by Potter et al. (1993).

3.3. Standardized anomaly index for NPP (SAI–NPP) for representing NPP anomalies

Standardized Anomaly Index (SAI), which was developed by Katz and Glantz (1986), was widely employed for evaluating the trends of precipitation (Hereford et al., 2002; Robertson et al., 2009; Nigrelli and Collimedaglia, 2012). This index was also applied effectively to the measurement of the anomalies of temperature (Giuffrida and Conte, 1989), NDVI (Peters et al., 2002) and snow cover (Valt and Cianfarra, 2010). For investigating NPP anomalies, we attempt to extend the SAI by taking China as a case study. Generally, the variance tends to increase as the mean NPP increases. Similarly, regions with high mean NPP values imply large NPP variances. In regions with high NPP gradients, there will be also high gradients in NPP variances. Considering the large gradients in NPP means and variances, regions with low NPP should receive higher weights for their comparability in different regions when reconstructing NPP anomalies. Thus, we assessed the NPP anomalies with SAI–NPP, which is defined as:

$$\mathrm{SAI}_{\mathrm{NPP}} = \frac{\mathrm{NPP}(i) - \overline{\mathrm{NPP}}}{\sigma_{\mathrm{NPP}}} \tag{15}$$

where $\mathrm{SAI}_{\mathrm{NPP}}$ is the NPP anomalies, namely SAI–NPP. NPP(i) is the amount of NPP in the year i; $\overline{\mathrm{NPP}}$ is the mean value of the NPP, and σ_{NPP} is the standard deviation of the NPP.

3.4. Assessing the impacts of droughts on NPP

3.4.1. Area-weighted drought intensity for the characterizations of droughts

While identifying the droughts, monthly SPI was calculated at different time scales (1, 3, 6, 9 and 12 months) based on the 31-year precipitation data (1980–2010) across China. After that, average SPI in the growing season (May to September) was computed as the annual SPI. The SPI corresponding to various land covers was then extracted based on the annual SPI by using GIS based on the distribution of several land covers (e.g. forest, shrubland, grassland, cropland, urban area and the sparse vegetation) in China.

For better measuring the deficits of precipitation, we investigated only drought-affected areas. In this paper, the drought-affected areas refer to those with a deficiency of precipitation, which was calculated as SPI < 0. Area-weighted drought intensity (AWDI), which represents the average severity of a drought in a region, was calculated by multiplying the SPI by the proportion of drought-affected areas in the total areas for each land covers in China. These calculations were implemented in the following way: (1) the drought-affected areas for various land covers were extracted based on the SPI and spatial distributions of several land covers in China; (2) average SPI was calculated to represent the mean drought intensity of each land cover; and (3) AWDI was calculated as a product of this average SPI and the proportion of drought-affected areas in the total areas of a certain land cover.

3.4.2. Representing NPP anomalies with SAI–NPP

Firstly, monthly NPP across China was modeled by using the CASA model. We then obtained annual NPP through the summation of the monthly values. The NPP anomalies was calculated with Eq. (15) based on the annual NPP from 2001 to 2010.

3.4.3. Evaluating the impacts of droughts on NPP

For exploring the relationships between drought severity and NPP, the SAI–NPP for various land covers was calculated separately based on the land covers data in China as well. Pearson correlation analysis was conducted between SAI–NPP and SPI at the time scales of 1, 3, 6, 9 and 12 months. Temporal dynamics of AWDI and the correlation coefficients R were then investigated at these scales as well. In addition, we analyzed the year-to-year variability of the SAI–NPP and the anomalies of some factors including droughts, NDVI, radiation, temperature.

4. Results

4.1. Validation of NPP and SAI–NPP

4.1.1. Validation of NPP

In this study, the distributions of NPP in China were modeled by using the CASA model. For verifying the reliability of the application of this model, we validated the model results based on Luo's (1996) investigation data and other literature. The plot sites that have the same vegetation types as the vegetation map were selected from Luo's (1996) investigation data. A significant correlation is found between our simulated NPP and observation–based data

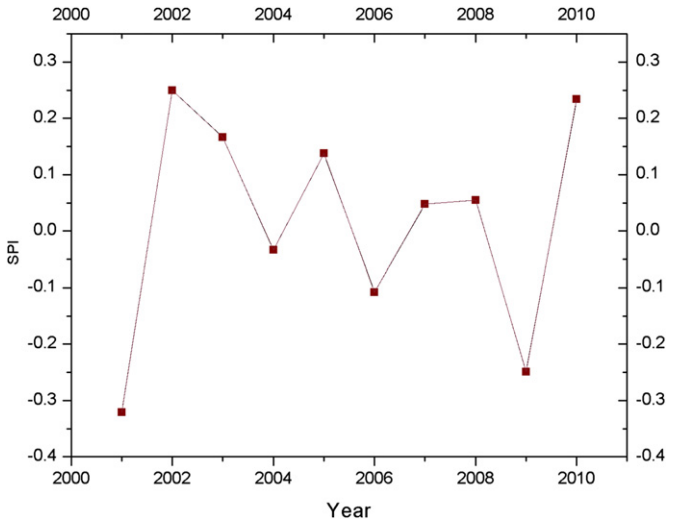

Fig. 1. Interannual variations of the SPI (wine squares) in China from 2001 to 2010.

($r = 0.733$, $P < 0.001$, $n = 248$). In addition, a comparison was conducted between our estimated NPP and other published summaries of NPP studies. According to our study, average annual NPP in China is 2.54 Pg C (1 Pg C = 10^{15} g C). This is within the reported values of 1.95–6.13 Pg C (Piao, 2001; Chen et al., 2001; Feng et al., 2007; Zhu et al., 2007). These indicate that the CASA is applicable to the modeling of the NPP across China.

4.1.2. Validation of SAI–NPP

Vegetation Health Index (VHI), which was developed by Kogan et al. (2004), provides combined characterizations of both moisture and thermal conditions while representing the vegetation health. It proved to be effective in monitoring the vegetation conditions (Kogan et al., 2011). Thus, we validated the SAI–NPP by performing correlation analysis between the SAI–NPP and the VHI based on time series of VHI data from 2001 to 2010. A significant correlation is noted between the SAI–NPP and the VHI ($r = 0.717$, $P = 0.020$, $n = 10$). This indicates the suitability of the SAI–NPP for representing the NPP anomalies in China.

4.2. Identification of the regional droughts in China

Since nearly half of the regions in China are located in monsoon climate zones, the water and heat energy is unevenly distributed in time and space. In the past decade (2001–2010), China witnessed several drought events, with different intensities and areal extents. In this paper, the obvious droughts that occurred in the years 2001, 2006 and 2009 were reconstructed by using SPI at the time scale of three months (Fig. 1). This is in accordance with the findings of Wang et al. (2011a,b) and Wu et al. (2011). The identification of these droughts indicates that SPI can be applied to the monitoring the droughts in China effectively.

As shown in Figs. 1 and 2, one of the most severe droughts during a 10-year period (2001–2010), which was caused by the persistent anomalous circulation over the Eurasia (Wei et al., 2004), occurred in the Northern China in 2001. During this drought period, the total drought-affected areas reached 6.46 million km^2, or 68% of land areas of the entire country. More concretely, severe/extreme drought areas covered approximately 0.74 million km^2, in comparison with the mild drought area of 5.72 million km^2 (approximately 7.84% and 60% of land areas of the entire country, respectively). In addition, the drought-affected areas covered approximately 7.02 million km^2 in 2009 (Figs. 1 and 4), accounting for about 74% of total land areas in China, which is larger than that in 2001. However, the severe/extreme drought areas were low, approximately 0.21 million km^2, and accounting for nearly 28% of that in 2001. In terms of drought intensity, the area-averaged SPI over China reached a value of −0.32 in 2001, which is also smaller than that in 2009 (approximately −0.25). All these indicate the occurrence of an extremely severe drought in 2001.

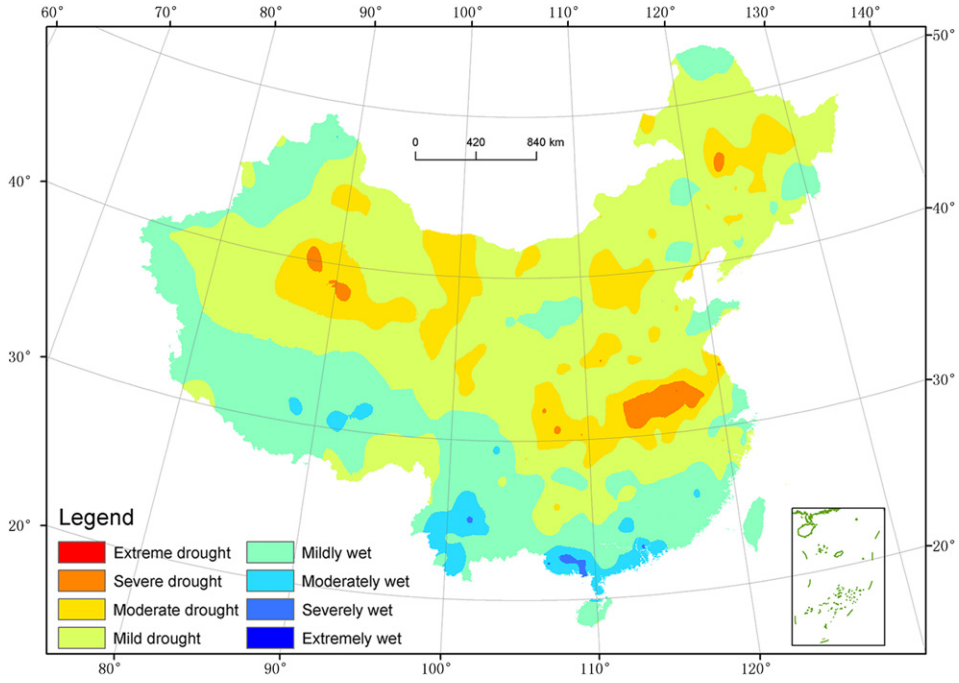

Fig. 2. Spatial distribution of the drought severity in China in 2001.

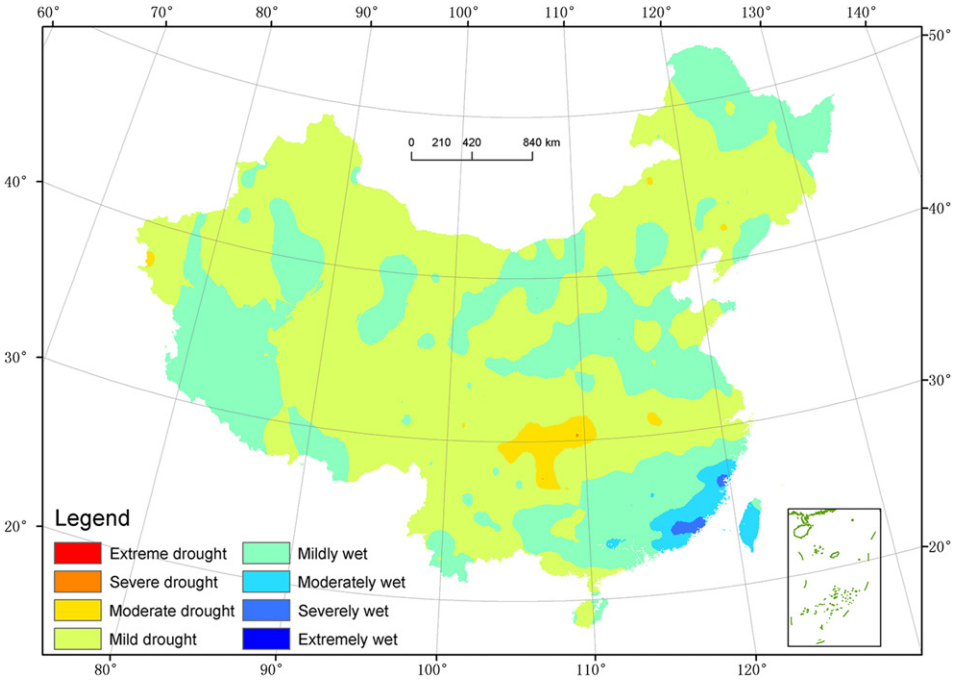

Fig. 3. The same as Fig. 2, but for the year 2006.

In 2006, the drought intensity was less serious than that in 2001 and 2009 (Fig. 1), with severe/extreme drought area of 0.05 million km^2. However, the mild drought areas reached 6.40 million km^2, which is comparable to that in the years 2001 and 2009. In addition, drought intensity in this year was found to be weak as well, with an averaged SPI value of −0.1. As to the spatial distribution, the drought in 2006, which caused a shortage of drinking water and affected the lives of more than 21 million people (Hao et al., 2007), mainly occurred around the regions of Chongqing-Sichuan area (Fig. 3).

4.3. Analyses of the impacts of droughts on NPP

For exploring the drought effects on NPP, the droughts in 2001 and 2009 were further investigated by performing several statistical analyses. Temporal variations of correlation coefficients R between the average SPI in the growing season and the annual SAI–NPP, as well as the AWDI were examined at time scales of 1, 3, 6, 9 and 12 months for this two years. In addition, NDVI and water supplying vegetation index (WSVI) proved to be good indicators of vegetation's ability (Xiao et al., 1995; Wang et al., 2003), and hence can regulate the carbon cycle, especially NPP (Imhoff et al., 2000). For validating our results, a comparison was made between our calculated correlation coefficients R and the correlations of other studies based on NDVI/WSVI. The correlation between NDVI and the SPI often fluctuates at different time scales. There are sometimes strong correlations between these two factors. However, in some cases, the correlation coefficients are even less than zero (Ji and Peters, 2003). Additionally, the correlation coefficients between SPI and WSVI vary between 0.022 and 0.697 (Jain et al., 2010). As shown in Tables 2 and 3, our estimated correlation coefficients R, which range from 0.05 to 0.44, are all within the reported values. This indicates the reliability of our results.

As to the drought intensity, various land covers suffered from a serious drought in China in 2001, with the minimal AWDI value of −0.77 at the time scale of six months (Table 2 and Fig. 2). In addition, the AWDI exerts continuous increases from the time scale of twelve months. It peaks at the time scale of six months for all the land covers, and then drops to low values at time scale of one month accounting for the precipitation deficits of the present month. These apparent trends of AWDI indicate the temporal variability of drought intensity in this country.

The drought in China in 2001 exerted remarkable effects on NPP as well. Significant positive correlations between SPI and SAI–NPP

Table 2
Variations of the correlation coefficients R and AWDI at different time scales in 2001 ($n_{forest} = 66082$, $n_{shrubland} = 38559$, $n_{grassland} = 117444$, $n_{cropland} = 74384$, $n_{urbanarea} = 1675$, $n_{sparsevegetation} = 83678$, $P < 0.0001$).

Land cover type	1 Month		3 Months		6 Months		9 Months		12 Months	
	R	AWDI	R	AWDI	R	AWDI	R	AWDI	R	AWDI
Forest	0.26	−0.30	0.31	−0.38	0.27	*−0.43*	0.28	−0.33	0.33	−0.29
Shrubland	0.20	−0.28	0.25	−0.38	0.24	*−0.43*	0.26	−0.34	0.28	−0.28
Grassland	0.35	−0.21	0.40	−0.37	0.38	*−0.44*	0.39	−0.42	0.40	−0.42
Cropland	0.32	−0.44	0.40	−0.63	0.39	*−0.70*	0.39	−0.51	0.34	−0.39
Urban area	0.21	−0.44	0.27	−0.58	0.26	*−0.62*	0.27	−0.41	0.25	−0.32
SparseVeg	0.20	−0.24	0.21	−0.60	0.21	*−0.77*	0.23	−0.77	0.22	−0.66

R represents the correlation between the average SPI in the growing season and the annual SAI–NPP.
AWDI represents the average severity of a drought in a region.
$N_{vegtype}$ is the amount of the cells when calculating R for various vegetation types.

Table 3
Variations of the correlation coefficients R and AWDI at different time scales in 2009 ($n_{forest} = 66082$, $n_{shrubland} = 38559$, $n_{grassland} = 117444$, $n_{cropland} = 74384$, $n_{urbanarea} = 1675$, $n_{sparsevegetation} = 83678$, $P < 0.0001$).

Land cover type	1 Month		3 Months		6 Months		9 Months		12 Months	
	R	AWDI	*R*	AWDI	*R*	AWDI	*R*	AWDI	*R*	AWDI
Forest	0.05	−0.20	0.08	−0.23	0.15	−0.30	0.15	*−0.30*	0.06	−0.29
Shrubland	0.07	−0.24	0.10	−0.27	0.07	*−0.33*	0.11	−0.29	0.09	−0.23
Grassland	0.40	−0.20	0.42	−0.32	0.31	*−0.38*	0.39	−0.36	0.44	−0.26
Cropland	0.34	−0.20	0.28	−0.22	0.18	*−0.24*	0.18	−0.24	0.17	−0.22
Urban area	0.17	−0.14	0.15	−0.16	0.10	−0.19	0.10	*−0.21*	0.12	−0.18
Sparse Veg	0.11	−0.19	0.14	−0.61	0.10	*−0.70*	0.14	−0.65	0.20	−0.50

Refer to Table 2 for the abbreviations details.

can be noted for all land covers (Table 3). The trends of these correlation coefficients R along with AWDI at different time scales are obvious in this year. That is, after the drought intensity (AWDI) peaks at the time scale of six months, the correlations achieve their maximum at the time scale of three months. This is available for most of the land covers, except for the sparse vegetation (six months) (Table 2).

As the indicator of droughts for various land covers, most of the AWDI values in 2009 are larger than that in 2001 (Tables 2 and 3), implying relatively low drought stresses in this period. The correlation coefficients R are smaller than that of the values in 2001, with a maximum of 0.42 for grassland at the time scale of three months. The drought intensity AWDI exhibits an obvious trend at different time scales as well. The drought in 2009, which is represented as AWDI, peaked at the time scales of six and nine months. This can be explained by the cumulative effects of precipitation deficits.

What's more, temporal trends of the combination of AWDI and correlation coefficients R along with the time scale are apparent for various land covers in 2009. Maximal R can be found after AWDI reaches their peak values (Table 3). More concretely, R peaks at the time scale of one month for cropland just after AWDI attains its maximum at the time scale of six months. Similar results can be found for the other land cover types. Similar to that in 2001, this can be attributed to the cumulative and lag effects of vegetation responses to the deficits of precipitation. Evidence can also be found in the findings of Ji and Peters (2003). This finding is crucial while monitoring the effects of droughts on NPP by using SPI.

Besides the temporal changes of the droughts itself and the relationships R between NPP anomalies and SPI, interannual variability of the NPP were investigated as well. During the past decade (2001–2010), the NPP over China exhibited an increase, from 2.25 Pg C in 2001 to 2.44 Pg C in 2010, with an average rate of 0.90% each year. As shown in Fig. 5, the NPP in China was anomalously low in 2001. The reduced NPP in 2001 could be associated with the cumulative effects of the serious drought that occurred during the period 1999–2002 (Wu et al., 2011).

As shown in Figs. 3 and 6, the drought in 2006 was mildness-dominated, with the mild drought-affected area of 6.35 million km^2, accounting for 67.07% of the land areas in the entire country. However, the annual NPP exhibited a slight increase as the drought occurred (Fig. 6). This indicates that mild droughts did not exhibit substantial limited effects on NPP. This kind of drought may even increase the plant growth in humid regions as fewer cloudiness which caused by droughts increases the incoming PAR (Xiao et al., 2009). In addition, the varied radiation and warm temperature can contribute to the increase in NPP as well.

Relatively high NPP (2.62 Pg C) can be found in 2009, despite an occurrence of a serious drought in this period (Figs. 1 and 4). This

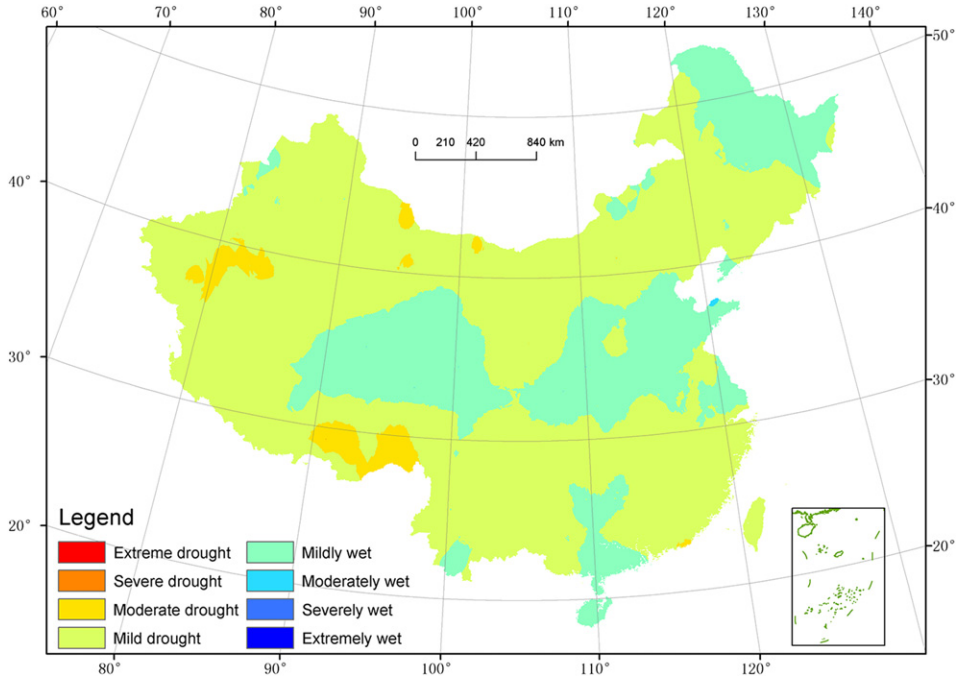

Fig. 4. The same as Fig. 2, but for the year 2009.

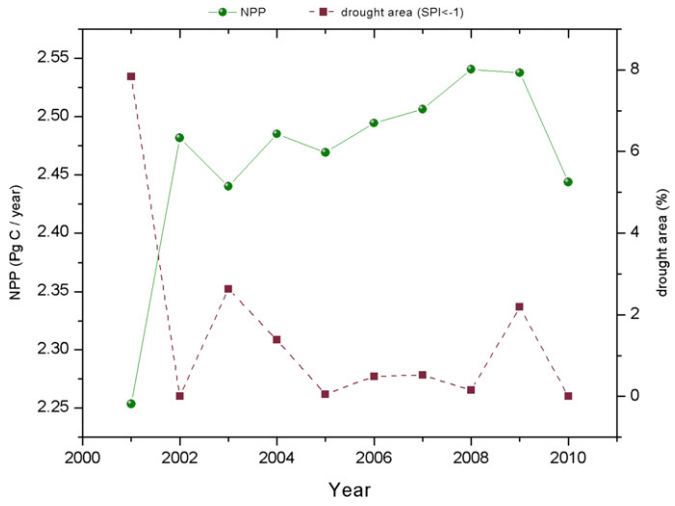

Fig. 5. Interannual variations of NPP (olive spheres) and drought areas (SPI < -1) (wine squares) in China from 2001 to 2010.

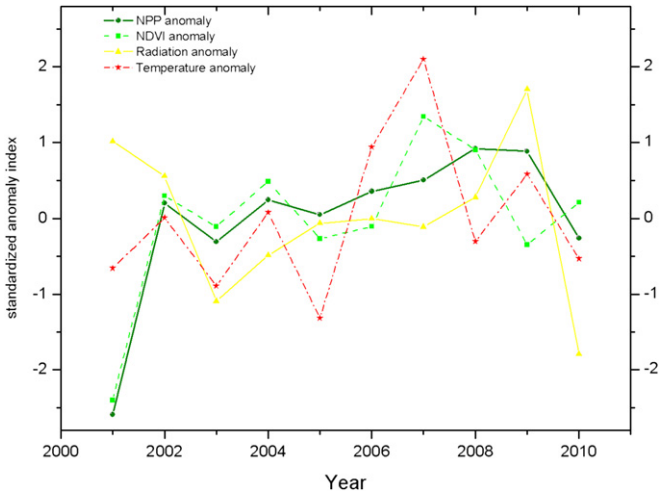

Fig. 7. Interannual variations from 2001 to 2010 in the anomalies of annual NPP (olive spheres), NDVI (green squares), radiation (yellow triangles) and temperature (red stars). (For interpretation of the references to color in this figure legend, the reader is referred to the web version of this article.)

phenomenon can be explained by the widespread distributions of mild drought areas (approximately 6.81 million km^2, accounting for 71.89% of the total land areas in China) and less severe/extreme drought areas (approximately 0.21 million km^2) (Figs. 5 and 6).

Temporal changes of NPP and droughts were also explored by performing a correlation analysis between NPP anomalies and the droughts expressed as SPI. As to the drought intensity, SPI values from −0.99 to 0.99 represent the near-normal conditions in relation to photosynthesis for vegetation (Table 1). Thus, we examined only the drought areas that SPI < -1 instead. As shown in Fig. 5, this drought area (SPI < -1) revealed a slight fluctuation from 2001 to 2010. Additionally, considerable year-to-year variability between NPP and the drought area (SPI < -1) are noted. The temporal variations of NPP are negatively correlated with the drought area that SPI < -1 ($r = -0.842$, $P = 0.002$, $n = 10$). This indicates that the serious droughts (SPI < -1) reduced the terrestrial NPP, whereas mild droughts ($-1 <$ SPI < 0) did not exhibit an obvious effect of reduction of the countrywide NPP. Particularly, the mild droughts could even increase NPP slightly in humid conditions by increasing the incoming PAR. This phenomenon was mainly associated with the drought intensity, drought duration and drought-affected areas. In addition to the drought conditions, the variability of NPP was probably caused by the combined effects of temperature, precipitation, radiation and so on. Thus, we further explored the interannual variability of the NPP and its relationships with the other climatic factors, including NDVI, radiation and temperature.

As shown in Fig. 7, the NPP in China increased slightly during the past decade (2001–2010). Interannual variations of NPP anomalies are correlated positively with the mean NDVI anomaly ($r = 0.838$, $P = 0.002$, $n = 10$). Although the radiation in 2001 was much higher than that in other years (Fig. 7), the NPP was lower in this period. This may be associating with the deficits of precipitation (Fig. 3). Thus, droughts, NDVI and radiation could be the crucial drivers of the temporal dynamics of NPP anomalies. In addition, the mean temperature rose slightly during this period (Fig. 7). However, the correlation between temperature and NPP anomalies is not significant ($r = 0.412$, $P = 0.237$, $n = 10$). This result coincides well with the results of Piao (2001).

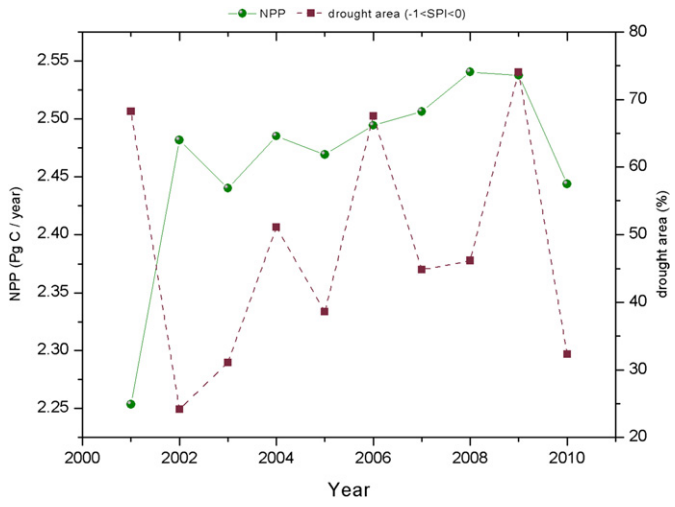

Fig. 6. The same as Fig. 5, but for $0 <$ SPI < -1.

5. Conclusions

In this article, the droughts in the years 2001, 2006 and 2009 were well reconstructed, indicating that SPI is suitable to monitor the droughts in China during the past decade (2001–2010). In addition, standardized anomaly index (SAI) was extended as SAI–NPP to represent the NPP anomalies effectively. According to our analysis to several droughts at multiple time scales, the time scale of SPI exhibiting the best correlations with NPP anomalies was not uniform for various vegetation types at anytime and anywhere. For instance, in 2001, the area-weighted drought intensity (AWDI) at the time scale of three months was found to have the best correlations with NPP anomalies for most of the land covers in China, except for the sparse vegetation (six months). However, for the year 2009, these high correlations could be obtained at times scales of one, three or six months. These correlations could be associated with the regional differentiation of drought intensity, drought duration and vegetation types. In addition, the strongest correlations between drought intensity and NPP anomalies could be found during or after the drought intensities reached their peak values. This can be explained by the cumulative and lag effects of vegetation responses to the deficits of precipitation. The findings are a crucial supplement to determine the time scale of SPI that correlated best with NPP anomalies while monitoring NPP. As to the

interannual variations, the NPP was anomalously low in 2001. This can be caused by the severe droughts in this year. Conversely, the NPP exhibited a slight increase as the mildness-dominated droughts occurred in 2006. This phenomenon implies that some droughts substantially reduced the countrywide NPP, whereas the others not. This uncertainty of the impacts on NPP was primarily associated with drought intensity, drought duration, drought-affected areas, as well as the cumulative and lag effects of the vegetation responses to the deficits of precipitation. In addition, NDVI, radiation and temperature could exert important influences as well. These findings should be significant for the monitoring of NPP anomalies associated with droughts while representing the droughts as SPI.

This article explored the NPP anomalies that were associated with droughts in China during the past decade by using SAI–NPP and SPI. The NPP responses in this analysis may help to clarify the impacts of droughts from other factors in the global carbon cycle, including climate change, deforestation and wildfire. However, a single factor cannot account for such complicated trends of the NPP anomalies, which are probably affected by the joint effects of various factors, such as temperature and precipitation. This paper does not investigate the combined contributions of these factors. Further studies are essential to quantify the influences of various factors (e.g. climate conditions, land covers and site-based factors) on NPP anomalies separately.

Acknowledgment

This study was supported by the National Basic Research Program of China (973 Program) (Grant No. 2011CB707103) and the Key National Natural Science Foundation of China (Grant No. 40830532).

References

Abramowitz, M., Stegun, I.A., 1964. Handbook of Mathematical Functions with Formulas, Graphs, and Mathematical Tables. Dover Publications, New York.

Arnone III, J.A., Verburg, P.S.J., Johnson, D.W., Larsen, J.D., Jasoni, R.L., Lucchesi, A.J., Batts, C.M., von Nagy, C., Coulombe, W.G., Schorran, D.E., Buck, P.E., Braswell, B.H., Coleman, J.S., Sherry, R.A., Wallace, L.L., Luo, Y., Schimel, D.S., 2008. Prolonged suppression of ecosystem carbon dioxide uptake after an anomalously warm year. Nature 455, 383–386.

Burke, E.J., Brown, S.J., Christidis, N., 2006. Modeling the recent evolution of global drought and projections for the twenty-first century with the Hadley Centre climate model. Journal of Hydrometeorology 7, 1113–1125.

Canadell, J.G., Le Quéré, C., Raupach, M.R., Field, C.B., Buitenhuis, E.T., Ciais, P., Conway, T.J., Gillett, N.P., Houghton, R.A., Marland, G., 2007. Contributions to accelerating atmospheric CO2 growth from economic activity, carbon intensity, and efficiency of natural sinks. Proceedings of the National Academy of Sciences of the United States of America 104, 18866.

Chen, L.J., Liu, G.H., Fen, X.F., 2001. Estimation of net primary productivity of terrestrial vegetation in China by remote sensing. Acta Botanica Sinica 43, 1191–1198.

Ciais, P., Reichstein, M., Viovy, N., Granier, A., Ogee, J., Allard, V., Aubinet, M., Buchmann, N., Bernhofer, C., Carrara, A., 2005. Europe-wide reduction in primary productivity caused by the heat and drought in 2003. Nature 437, 529–533.

Cramer, W., Kicklighter, D.W., Bondeau, A., Iii, B.M., Churkina, G., Nemry, B., Ruimy, A., Schloss, A.L., 1999. Comparing global models of terrestrial net primary productivity (NPP): overview and key results. Global Change Biology 5, 1–15.

Editorial Board of Vegetation Map of China, 2001. Vegetation Atlas of China(1: 1000000). Science Press, Beijing.

Fan, S., Gloor, M., Mahlman, J., Pacala, S., Sarmiento, J., Takahashi, T., Tans, P., 1998. A large terrestrial carbon sink in North America implied by atmospheric and oceanic carbon dioxide data and models. Science 282, 442.

Fang, J.Y., Guo, Z.D., Piao, S.L., Chen, A.P., 2007. Terrestrial vegetation carbon sinks in China, 1981–2000. Science in China Series D: Earth Sciences 50, 1341–1350.

Feng, X., Liu, G., Chen, J.M., Chen, M., Liu, J., Ju, W.M., Sun, R., Zhou, W., 2007. Net primary productivity of China's terrestrial ecosystems from a process model driven by remote sensing. Journal of Environmental Management 85, 563–573.

Fernandes, D.S., Heinemann, A.B., 2011. Rice yield variability estimates at different time scales of SPI index. Pesquisa Agropecuária Brasileira 46, 335–343.

Freddy, N., Harrij, V.V., Luc, V., 2008. Harmonized World Soil Database. Food and Agriculture Organization of the United Nations.

Fung, I.Y., Doney, S.C., Lindsay, K., John, J., 2005. Evolution of carbon sinks in a changing climate. Proceedings of the National Academy of Sciences of the United States of America 102, 11201.

Giuffrida, A., Conte, M., 1989. Long term evolution of the italian climate outlined by using the standardized anomaly index (SAI). In: Conference on Climate and Water, pp. 197–208 (Helsinki Finland).

Goodale, C.L., Apps, M.J., Birdsey, R.A., Field, C.B., Heath, L.S., Houghton, R.A., Jenkins, J.C., Kohlmaier, G.H., Kurz, W., Liu, S., 2002. Forest carbon sinks in the Northern Hemisphere. Ecological Applications 12, 891–899.

Gregory, J.M., Mitchell, J.F.B., Brady, A.J., 1997. Summer drought in northern midlatitudes in a time-dependent CO2 climate experiment. Journal of Climate 10, 662–686.

Hao, Z., Ge, Q., Zheng, J., Li, Y., 2007. 2006 extreme drought event of Chongqing. Geographical Research, 4.

Hereford, R., Webb, R.H., Graham, S., 2002. In: Hendley II, J.W., Stauffer, P.H. (Eds.), Precipitation History of the Colorado Plateau Region, 1900–2000. US Department of the Interior, US Geological Survey.

Houghton, R.A., Goodale, C.L., 2004. Effects of land-use change on the carbon balance of terrestrial ecosystems. Ecosystems and Land Use Change 10, 85–98.

Imhoff, M.L., Tucker, C.J., Lawrence, W.T., Stutzer, D.C., 2000. The use of multisource satellite and geospatial data to study the effect of urbanization on primary productivity in the United States. IEEE Transactions on Geoscience and Remote Sensing 38, 2549–2556.

IPCC, 2007. Climate Change 2007: synthesis report. In: Bernstein, L., Reisinger, A., Riahi, K., Bosch, P. (Eds.), Contribution of Working Groups I, II and III to the Fourth Assessment Report of the Intergovernmental Panel on Climate Change, p. 49.

Jain, S., Keshri, R., Goswami, A., Sarkar, A., 2010. Application of meteorological and vegetation indices for evaluation of drought impact: a case study for Rajasthan, India. Natural Hazards 54, 643–656.

Ji, L., Peters, A.J., 2003. Assessing vegetation response to drought in the northern Great Plains using vegetation and drought indices. Remote Sensing of Environment 87, 85–98.

Jin, Z., Qi, Y.C., Dong, Y.S., 2007. Storage of biomass and net primary productivity in desert shrubland of Artemisia ordosica on Ordos Plateau of Inner Mongolia, China. Journal of Forestry Research.

Katz, R.W., Glantz, M.H., 1986. Anatomy of a rainfall index. Monthly Weather Review 114, 764–771.

Kogan, F., Stark, R., Gitelson, A., Jargalsaikhan, L., Dugrajav, C., Tsooj, S., 2004. Derivation of pasture biomass in Mongolia from AVHRR-based vegetation health indices. International Journal of Remote Sensing 25, 2889–2896.

Kogan, F., Adamenko, T., Kulbida, M., 2011. Satellite-based crop production monitoring in Ukraine and regional food security. Use of Satellite and In-Situ Data to Improve Sustainability, 99–104.

Kurz, W.A., Stinson, G., Rampley, G.J., Dymond, C.C., Neilson, E.T., 2008. Risk of natural disturbances makes future contribution of Canada's forests to the global carbon cycle highly uncertain. Proceedings of the National Academy of Sciences of the United States of America 105, 1551.

Li, X., 1998. Measurement of rapid agricultural land loss in the Pearl River Delta with the integration of remote sensing and GIS. Environment and Planning B: Planning and Design 25, 447–461.

Liu, W.T., Juárez, R.I.N., 2001. ENSO drought onset prediction in northeast Brazil using NDVI. International Journal of Remote Sensing 22, 3483–3501.

Lloyd Hughes, B., Saunders, M.A., 2002. A drought climatology for Europe. International Journal of Climatology 22, 1571–1592.

Lobell, D.B., Hicke, J.A., Asner, G.P., Field, C.B., Tucker, C.J., Los, S.O., 2002. Satellite estimates of productivity and light use efficiency in United States agriculture, 1982–98. Global Change Biology 8, 722–735.

Luo, T.X., 1996. Patterns of net primary productivity for Chinese major forest types and its mathematical models. Chinese Academy of Sciences.

McKee, T.B., Doesken, N.J., Kleist, J., 1993. The relationship of drought frequency and duration to time scales. In: Eighth Conference on Applied Climatology. American Meteorological Society Boston, MA, Anaheim, California.

Myneni, R.B., Dong, J., Tucker, C.J., Kaufmann, R.K., Kauppi, P.E., Liski, J., Zhou, L., Alexeyev, V., Hughes, M.K., 2001. A large carbon sink in the woody biomass of northern forests. Proceedings of the National Academy of Sciences of the United States of America 98, 14784.

Ni, J., 2004. Estimating net primary productivity of grasslands from field biomass measurements in temperate northern China. Plant Ecology 174, 217–234.

Nigrelli, G., Collimedaglia, M., 2012. Reconstruction and analysis of two long-term precipitation time series: Alpe Devero and Domodossola (Italian Western Alps). Theoretical and Applied Climatology, 1–9.

Palmer, W.C., Bureau, E.U.W., 1965. Meteorological Drought. US Weather Bureau, Washington, DC.

Peters, A.J., Walter-Shea, E.A., Ji, L., Vina, A., Hayes, M., Svoboda, M.D., 2002. Drought monitoring with NDVI-based standardized vegetation index. Photogrammetric Engineering and Remote Sensing 68, 71–75.

Peylin, P., Baker, D., Sarmiento, J., Ciais, P., Bousquet, P., 2002. Influence of transport uncertainty on annual mean and seasonal inversions of atmospheric CO2 data. Journal of Geophysical Research-Atmospheres 107.

Piao, S.L., 2001. Application of CASA model to the estimation of Chinese terrestrial net primary productivity. Acta Phytoecologica Sinica 25, 603–608.

Piao, S.L., Fang, J.Y., Zhou, L.M., Zhu, B., Tan, K., Tao, S., 2005. Changes in vegetation net primary productivity from 1982 to 1999 in China. Global Biogeochemical Cycles 19.

Pickett, S.T.A., White, P.S., 1986. The Ecology of Natural Disturbance and Patch Dynamics. Academic Press, New York.

Potter, C.S., Randerson, J.T., Field, C.B., Matson, P.A., Vitousek, P.M., Mooney, H.A., Klooster, S.A., 1993. Terrestrial ecosystem production: a process model based on global satellite and surface data. Global Biogeochemical Cycles 7 (4), 811–841.

Potter, C., TAN, P.N., Steinbach, M., Klooster, S., Kumar, V., Myneni, R., Genovese, V., 2003. Major disturbance events in terrestrial ecosystems detected using global satellite data sets. Global Change Biology 9, 1005–1021.

Robertson, A.W., Moron, V., Swarinoto, Y., 2009. Seasonal predictability of daily rainfall statistics over Indramayu district, Indonesia. International Journal of Climatology 29, 1449–1462.

Running, S.W., 2008. Ecosystem disturbance, carbon, and climate. Science 321, 652–653.

Sato, H., Itoh, A., Kohyama, T., 2007. SEIB-DGVM: A new dynamic global vegetation model using a spatially explicit individual-based approach. Ecological Modelling 200, 279–307.

Sitch, S., Smith, B., Prentice, I.C., Arneth, A., Bondeau, A., Cramer, W., Kaplan, J.O., Levis, S., Lucht, W., Sykes, M.T., 2003. Evaluation of ecosystem dynamics, plant geography and terrestrial carbon cycling in the LPJ dynamic global vegetation model. Global Change Biology 9, 161–185.

Stephens, B.B., Gurney, K.R., Tans, P.P., Sweeney, C., Peters, W., Bruhwiler, L., Ciais, P., Ramonet, M., Bousquet, P., Nakazawa, T., 2007. Weak northern and strong tropical land carbon uptake from vertical profiles of atmospheric CO2. Science 316, 1732.

Togtohyn, C., Ojima, D., 1996. NPP Grassland: Tumentsogt, Mongolia, 1982–1990. Oak Ridge National Laboratory Distributed Active Archive Center, Tennessee, USA.

Tsakiris, G., Vangelis, H., 2005. Establishing a Drought Index incorporating evapotranspiration. European Water 9, 3–11.

Valt, M., Cianfarra, P., 2010. Recent snow cover variability in the Italian Alps. Cold Regions Science and Technology 64, 146–157.

van der Werf, G.R., Randerson, J.T., Giglio, L., Collatz, G.J., Mu, M., Kasibhatla, P.S., Morton, D.C., DeFries, R.S., Jin, Y., van Leeuwen, T.T., 2010. Global fire emissions and the contribution of deforestation, savanna, forest, agricultural, and peat fires (1997–2009). Atmospheric Chemistry and Physics 10, 11707–11735.

Wang, J., Rich, P.M., Price, K.P., 2003. Temporal responses of NDVI to precipitation and temperature in the central Great Plains, USA. International Journal of Remote Sensing 24, 1–2204.

Wang, A., Lettenmaier, D.P., Sheffield, J., 2011a. Soil moisture drought in China, 1950–2006. Bulletin of the American Meteorological Society 7, 3257–3271.

Wang, G.L., Wu, B., Jia, C.L., Yang, Q.L., Sheng, Y.B., 2011b. Grassland vegetation characteristics of shrub-grass land in Wufeng Mountain Area of Ji'nan City. Bulletin of Soil and Water Conservation 31, 228–237.

Wei, J., Zhang, Q., Tao, S., 2004. Physical causes of the 1999 and 2000 Summer Severe Drought in North China. Chinese Journal of Atmospheric Sciences 1, 125–137.

Weng, Q., 2002. Land use change analysis in the Zhujiang Delta of China using satellite remote sensing, GIS and stochastic modelling. Journal of Environmental Management 64, 273–284.

Wu, Z.Y., Lu, G.H., Wen, L., Lin, C.A., 2011. Reconstructing and analyzing China's fifty-nine year (1951–2009) drought history using hydrological model simulation. Hydrology and Earth System Sciences Discussions 8, 1861–1893.

Xiao, Q., Chen, W., Liang, G., Du, P., 1995. A study on drought monitoring using meteorological satellite data. In: Technical Reports of National Satellite Meteorological Centre, pp. 9509–9519.

Xiao, J., Zhuang, Q., Liang, E., Shao, X., McGuire, A.D., Moody, A., Kicklighter, D.W., Melillo, J.M., 2009. Twentieth-century droughts and their impacts on terrestrial carbon cycling in China. Earth Interactions 13, 1–31.

Xu, C., Liu, M., An, S., Chen, J.M., Yan, P., 2007. Assessing the impact of urbanization on regional net primary productivity in Jiangyln County, China. Journal of Environmental Management 85, 597–606.

Yu, Y.W., Hu, Z.Z., Zhang, D.G., Xu, C.L., 2000. The net primary productivity of potentilla fruticosa shrub. Acta Prataculturae Sinica 9, 33–39.

Zeng, N., Qian, H., Munoz, E., Iacono, R., 2004. How strong is carbon cycle-climate feedback under global warming. Geophysical Research Letters 31.

Zhao, M., Running, S.W., 2010. Drought-induced reduction in global terrestrial net primary production from 2000 through 2009. Science 329, 940.

Zhu, W., Pan, Y., He, H., Yu, D., Hu, H., 2006. Simulation of maximum light use efficiency for some typical vegetation types in China. Chinese Science Bulletin 51, 457–463.

Zhu, W.Q., Pan, Y.Z., Zhang, J.S., 2007. Estimation of net primary productivity of Chinese terrestrial vegetation based on remote sensing. Journal of Plant Ecology 31, 413–424.